Articles

Identification of the Structural and Functional Boundaries of the Multidrug Resistance Protein 1 Cytoplasmic Loop 3†

Christopher J. Westlake,[‡,§] Yue-Ming Qian,[§,||] Mian Gao,[§] Monika Vasa,[§] Susan P. C. Cole,[§,⊥] and Roger G. Deeley*[,§,⊥]

Departments of Biochemistry and Pathology and Molecular Medicine and Cancer Research Institute, Queen's University, Kingston, Ontario, Canada K7L 3N6, and Department of Medicine, The Upstate Medical University, The State University of New York, Syracuse, New York 13210

Received July 25, 2003; Revised Manuscript Received September 26, 2003

ABSTRACT: Multidrug resistance protein (MRP) 1 is a member of the ABCC branch of the ATP binding cassette (ABC) transporter superfamily that can confer resistance to natural product chemotherapeutic drugs and transport a variety of conjugated organic anions, as well as some unconjugated compounds in a glutathione- (GSH-) dependent manner. In addition to the two tandemly repeated polytopic membrane-spanning domains (MSDs) typical of ABC transporters, MRP1 and its homologues MRP2, -3, -6, and -7 contain a third NH_2-terminal MSD. The cytoplasmic loop (CL3) connecting this MSD, but apparently not the MSD itself, is required for MRP1 leukotriene C_4 (LTC_4) transport activity, substrate binding and appropriate trafficking of the protein to the basolateral membrane. We have used a baculovirus dual-expression system to produce various functionally complementing fragments of MRP1 in insect Sf21 cells to precisely define the region in CL3 that is required for activity and substrate binding. Using a parallel approach in polarized MDCK-I cells, we have also defined the region of CL3 that is required for basolateral trafficking. The CL3 NH_2- and COOH-proximal functional boundaries have been identified as Cys^{208} and Asn^{260}, respectively. Cys^{208} also corresponds to the NH_2-proximal boundary of the region required for basolateral trafficking in MDCK-I cells. However, additional residues downstream of the CL3 COOH-proximal functional boundary extending to Lys^{270} were found to be important for basolateral localization. Finally, we show that regions in CL3 necessary for LTC_4 binding and transport are also required for binding of the photoactivatable GSH derivative azidophenacyl-GSH.

Multidrug resistance (MDR)[1] is a frequent cause of chemotherapy failure in cancer patients. The drug efflux pumps P-glycoprotein (P-gp) and multidrug resistance protein (MRP) 1 have been frequently implicated in MDR in vitro (*1*−*3*) and clinically in some forms of cancer (*4*). Both proteins are members of the ATP binding cassette (ABC) transporter superfamily. P-gp (ABCB1) and MRP1 (ABCC1) increase resistance to similar but not identical spectra of natural product drugs, including vinca alkaloids, epipodophyllotoxins, and anthracyclines (*1*, *5*, *6*). MRP1 is also capable of actively transporting a wide range of organic glutathione (GSH), glucuronate, and sulfate conjugates in vitro that are not substrates of P-gp. These include such structurally diverse compounds as leukotriene C_4 (LTC_4), 17β-estradiol-17-β-D-glucuronide ($E_2$17βG), glutathionylated aflatoxin B_1 epoxide, and GSSG (*7*−*11*), as well as some drug conjugates, such as etoposide−glucuronide (*9*), while GSH conjugates of doxorubicin and daunorubicin are effective inhibitors of LTC_4 transport (*12*). In addition to being ATP-dependent, transport of some MRP1 substrates is stimulated by GSH and a number of its nonreducing analogues, such as methyl-GS and ophthalmic acid (*13*−*15*). GSH-dependent substrates include some unconjugated drugs to which MRP1 confers resistance, such as vincristine and daunorubicin (*13*, *16*−*18*), as well as certain anionic

† This work was supported by a grant from the National Cancer Institute of Canada with funds from the Terry Fox Foundation. C.J.W. is the recipient of an Ontario Graduate Scholarship. S.P.C.C. is the Canada Research Chair in Cancer Biology, and R.G.D. is the Stauffer Professor of Basic Oncology at Queen's University.

* To whom correspondence should be addressed: Tel 613-533-2981; fax 613-533-6830; e-mail deeleyr@post.queensu.ca.

‡ Department of Biochemistry, Queen's University.

§ Cancer Research Institute, Queen's University.

|| SUNY.

⊥ Department of Pathology and Molecular Medicine, Queen's University.

[1] Abbreviations: MDR, multidrug resistance; MRP, multidrug resistance protein; P-gp, P-glycoprotein; CFTR, cystic fibrosis transmembrane conductance regulator; MSD, membrane-spanning domain; TM, transmembrane; NBD, nucleotide binding domain; CL3, cytoplasmic loop 3; MAb, monoclonal antibody; AG-A, agosterol-A; LTC_4, leukotriene C_4; GSH, glutathione; NADPH, reduced nicotinamide adenine dinucleotide phosphate; EDTA, ethylenediaminetetraacetic acid; PBS, phosphate-buffered saline; RT, room temperature; SDS−PAGE, sodium dodecyl sulfate−polyacrylamide gel electrophoresis; MDCK, Madin-Darby canine kidney; HEK, human embryonic kidney; β-gus, β-glucuronidase; MCS, multicloning site; PCR, polymerase chain reaction; pFB, pFastBac; SUR, sulfonylurea receptor.

10.1021/bi035333y CCC: $25.00
Published on Web 11/12/2003

conjugates, including estrone sulfate and the tobacco smoke carcinogen 4-(methylnitrosamino)-1-(3-pyridyl)-1-butanol (NNAL) *O*-glucuronide (*14*, *15*).

Six human homologues of MRP1 have been described, MRPs 2−7, (*19*−*21*), and two additional, more distantly related proteins have been identified in EST databases (*22*, *23*). Together with CFTR and the sulfonylurea receptors, these proteins comprise the ABCC branch of the superfamily. Unlike the majority of ABC transporters, MRPs 1, 2, 3, 6, and 7 have a third NH_2-terminal membrane-spanning domain (MSD) that appears to contain five TM helices (*24*, *25*). Thus these proteins have three tandemly arranged MSDs predicted to contain five, six, and six TM helices, respectively (*24*, *26*, *27*). The function of MSD1 in MRPs 1, 2, 3, 6, and 7 is currently unknown, and sequence conservation in this region is relatively low when compared with the level of homology of the core MSDs of the ABCC family members (*28*). In MRP1, the NH_2-proximal end of cytoplasmic loop (CL)3 connecting MSD1 to MSD2, is encoded by the 5′-end of exon 6 (*29*). This small region of the loop is relatively conserved among ABCC proteins with three MSDs and it aligns with the NH_2-termini of ABCC proteins that lack such a domain (e.g., MRP4, MRP5, and CFTR) (*29*).

Previously, we have shown that MRP1 proteins lacking the NH_2-proximal 228 or 280 amino acids, which includes MSD1 and parts of CL3, were unable to transport LTC_4. Transport could be rescued by coexpression of a polypeptide containing the first 280 amino acids of MRP1 with either truncated form of the protein but not by a fragment containing amino acids 1−227 (*30*). Internal deletions within CL3 have also been shown to inactivate MRP1 (*30*, *31*). In contrast, MRP1 truncated to amino acid 204, which leaves almost all of CL3 intact but eliminates MSD1, can bind (*32*) and transport LTC_4 (*33*, *34*) and traffics appropriately to the basolateral membrane in polarized cells (*33*). Furthermore, coexpression of a peptide containing CL3 amino acids 204−280 with an MRP1 fragment lacking the first 280 amino acids has been reported to reconstitute LTC_4 transport and to restore trafficking to the basolateral membrane (*31*).

The high-affinity MRP1 substrate LTC_4 photolabels sites in MSD2 and, to a lesser extent, MSD3. Although CL3 is not a site of labeling, it is required for photolabeling of sites in both MSDs (*32*). MRP1 can also be labeled by the structurally unrelated photoreactive azidoderivatized quinoline *N*-(hydrocinchonidin-8′-yl)-4-azido-2-hydroxybenzam (IACI) and the rhodamine 123 analogue iodoaryl azidorhodamine 123 (IAARh123) (*35*−*37*). Both compounds label sites in the COOH-proximal two TM helices of MSD2 and MSD3, and labeling can be competed by LTC_4. Neither compound photolabels CL3, although more recent studies indicate that CL3 is required for binding of IAARh123 (*37*). CL3 has also been found to be essential for the binding and photolabeling of MRP1 by the azido derivative of agosterol A (AG-A) and LY475776, agents that can reverse resistance mediated by MRP1 (*34*, *38*). Both azido-AG-A and LY475776 display very strong dependence on GSH for binding, and both compounds selectively label sites in the COOH-proximal half of the protein (*34*, *38*, *39*).

The lack of photolabeling of the NH_2-proximal half of the protein by AG-A has prompted the suggestion that CL3 may be involved in GSH binding (*34*). Recently, we demonstrated that MRP1 can be photolabeled with the GSH derivative *S*-(4-azidophenacyl)glutathione, which can substitute functionally for free GSH in supporting the transport of estrone sulfate (*38*). As found with LTC_4, azidophenacyl-GSH labeled both MSD2 and MSD3 of MRP1. In addition, photoaffinity labeling was dependent on the presence of the NH_2-terminal 280 amino acids, but as observed with LTC_4, this fragment was not a site of photolabeling (*38*). To further define the region of CL3 required for substrate binding and transport, and to examine its possible role in protein folding and trafficking, we have mapped both NH_2- and COOH-proximal functional boundaries by coexpression of MRP1 fragments in insect cells. We have also determined whether the functional boundaries defined by loss of transport activity in insect cells coincide with boundaries that define the ability of the protein to traffic appropriately in polarized mammalian cells.

MATERIALS AND METHODS

Materials. [14,15(n)-$^3H_2$]-LTC_4 (38 Ci mmol^{-1}) and fluorographic reagent Amplify were purchased from Amersham Pharmacia Biotech (Oakville, Ontario, Canada). [14,15,19,20-$^3H_4$]-LTC_4 (182 Ci mmol^{-1}) and [^{35}S]-GSH were from NEN Life Science Products (Boston, MA). LTC_4, 4-azidophenacylbromide, GSH reductase, NADPH, and digitonin were purchased from Calbiochem (La Jolla, CA); nucleotides, propidium iodide, RNaseA, and anti-calnexin MAb were from Sigma Chemical Co. (St. Louis, MO); and paraformaldehyde was from JBS Supplies (Dorval, Quebec, Canada). MAb MRPr1 was obtained from Alexis (San Diego, CA), and 7-aminoactinomycin D and fluorescent labeled secondary antibodies Alexa 488 and Alexa 546 were purchased from Molecular Probes (Eugene, OR). Canine Na^+/K^+-ATPase polyclonal antibody was purchased from ABCAM (abcam.com). Hygromycin B, Fugene6, and Complete EDTA-free protease inhibitors were purchased from Roche (Indianapolis, IN). Geneticin was obtained from Invitrogen Corporation (Burlington, Ontario, Canada).

Generation of MRP1 Constructs. Full-length MRP1 in the pFastBac (pFB) vector (pFB-MRP1) and pBluescript KS+ vector (pBSMRP-fc-ATG) and MRP1 fragments pFB-$MRP1_{1-281}$ and pFB-$MRP1_{281-1531}$ have been previously described (*6*, *30*, *40*). PCR was used to generate constructs lacking the NH_2-proximal region of MRP1 (Figure 1B) with pFB-MRP1 as a template. Forward primers designed for ΔN-CL3 MRP1 constructs contained an *Eag*I site followed by an initiator methionine codon within an *Nco*I site upstream from the coding sequence for MRP1. NH_2-terminally truncated constructs were designed to start translation at MRP1 amino acids 204, 208, 210, and 213. An additional codon (valine) was incorporated after the initiator methionine in the aa 208 truncation construct to retain the *Nco*I site. The reverse primer was located immediately downstream of a unique *Bam*HI site in the MRP1 coding sequence (nucleic acids 883−864). The NH_2-terminal coding region up to the *Bam*HI site was excised from the pBSMRP-fc-ATG vector by *Eag*I−*Bam*HI digestion and the approximately 200 bp MRP1 NH_2-truncation PCR fragments were inserted. The fidelity of the PCR reaction was confirmed by sequencing. The ΔN-CL3 MRP1 constructs were then excised by *Sac*I−*Kpn*I digestion and transferred into the pFB vector. In addition, the ΔN-CL3 MRP1 constructs in pFB, including pFB-$MRP1_{281-1531}$, were moved into the mammalian expres-

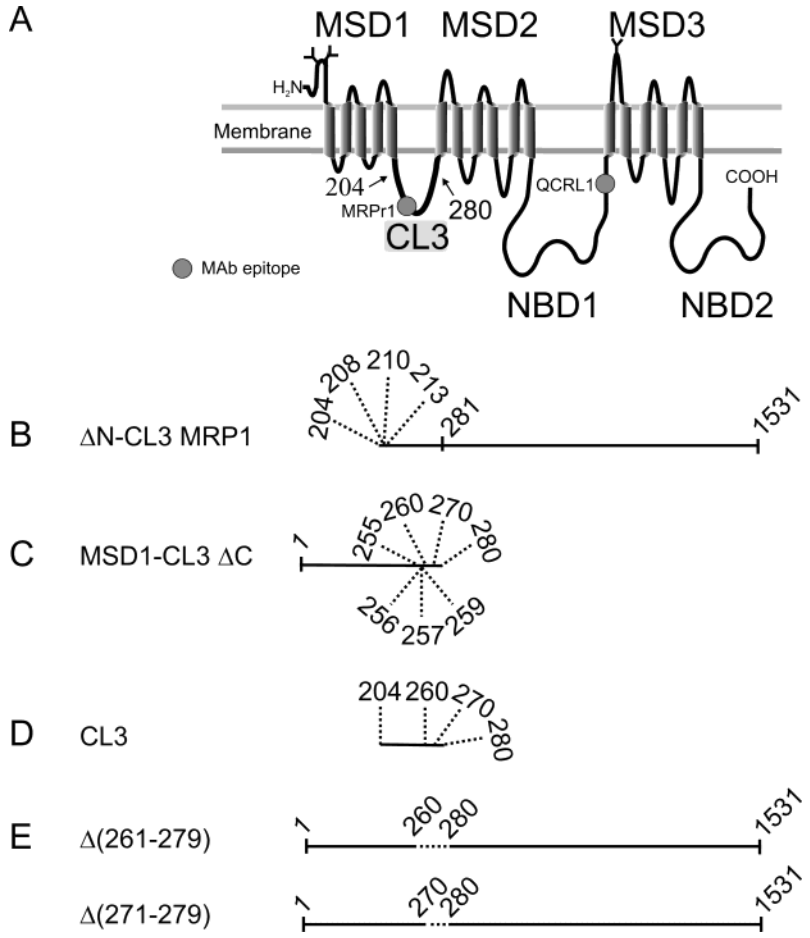

FIGURE 1: Illustration of MRP1 constructs generated. (A) Schematic representation of MRP1 (1−1531) in the plasma membrane based on computer-assisted hydropathy analysis. Locations of mapped antibody epitopes are indicated. (B−E) MRP1 constructs engineered by PCR.

sion vector pCDNA3.1(−) via an *Eag*I−*Kpn*I digest of the pFB DNA and *Not*I−*Kpn*I digestion of the vector.

A second mammalian expression vector, pCEBV7NL, that replicates episomally was modified to facilitate cloning of MRP constructs by introduction of a new expanded multicloning site (MCS). Briefly, the MCS from pCEBV7 vector (*41*) was excised by *Kpn*I−*Bam*HI digestion and the vector backbone was rendered blunt-ended. Sense and antisense oligonucleotides synthesized to create the new MCS were annealed and ligated into the vector backbone. The fidelity of the new MCS was confirmed by DNA sequencing. The ΔN-CL3 MRP1 constructs were then cloned into pCEBV7NL as described for pcDNA3.1(−).

MSD1 CL3-ΔC constructs (Figure 1C) were generated by PCR with a forward primer upstream of the *Pvu*II site in MSD1 and reverse primers that added a stop codon and an *Sph*I site after MRP1 codons for aa 255, 256, 257, 259, 260, 270, and 280. *Pvu*II−*Sph*I-digested PCR products were then inserted into *Pvu*II−*Sph*I-digested pFB-MRP1$_{1-281}$. All constructs were confirmed by sequencing. Finally, MSD1 CL3-ΔC constructs were subcloned, along with MRP1$_{281-1531}$, into the pFB DUAL expression vector. The pFB-MRP1$_{281-1531}$ construct was digested with *Sal*I (made blunt)−*Kpn*I, and this 3.9 kb MRP1 fragment was ligated into the MCS2 of the dual-expression vector, which had been digested *with Sma*I−*Kpn*I. MSD1 CL3-ΔC constructs in pFB were then inserted into MSC1 after *Hin*dIII (made blunt)−*Sac*I digestion of the pFB constructs and *Xba*I (made blunt)−*Sal*I digestion of the pFB DUAL MRP1$_{281-1531}$ vector.

Mammalian dual expression of MSD1 CL3-ΔC constructs with MRP1$_{281-1531}$ was achieved with the pMG-H2 vector (InvivoGen, San Diego, CA). The MRP1$_{281-1531}$ fragment in pCEBV7NL was excised by *Eag*I (made blunt)−*NheI* digestion and ligated into MCS1 of the vector via *Sma*I−*Xba*I. To facilitate cloning into MCS2 of pMG-H2, MSD1 CL3-ΔC MRP1 fragments were first excised from pFB by an *Eag*I−*Kpn*I digestion and ligated into *Not*I−*Kpn*I sites in pCEBV7NL. These fragments were then excised from pCEBV7NL by *Eag*I (made blunt)−*Nhe*I and inserted into *Sgr*AI−*Nhe*I-digested MCS2.

For constructs containing CL3 fragments alone (Figure 1D), the ΔN-CL3 MRP1 constructs in pFB were first digested with *Pfl*MI−*Avr*II to remove the COOH-proximal MRP1 nucleotides and a portion of the downstream vector sequence. The COOH-terminal sequence from MSD1 CL3-ΔC constructs cloned into pFB (*Pfl*MI−*Avr*II fragments) were then added back to the appropriate vector to make MRP1 204−260, 204−270, and 204−280. The completed CL3 constructs were also subcloned into the pFB DUAL expression vectors along with the MRP1$_{281-1531}$ construct as previously described for MSD1 CL3-ΔC constructs. In addition, to determine the subcellular localization of the CL3 peptides, pFB DUAL expression vectors containing the CL3 constructs and the β-glucuronidase gene (β-gus) (Invitrogen, San Diego, CA) were constructed.

MRP1 deletion constructs Δ(261−279) and Δ(271−279) were engineered with the T7 primer from the pBS-fc ATG MRP1 vector and reverse primers that contained sequence

up to and including codons for CL3 amino acids Asn^{260} or Lys^{270}, respectively, followed by a *Bam*HI site. Amplified fragments were cloned into *Eag*I−*Bam*HI-digested pFB-MRP1 vector. The assembled MRP1 CL3 deletion constructs were further subcloned into pcDNA3.1(−) as described for ΔN-CL3 MRP1.

Recombinant Baculovirus Production and Viral Infection. Transformation of donor pFB and pFB DUAL plasmid constructs, isolation of recombinant bacmids, and subsequent transfection into Sf21 cells were as described previously (*40*). High-titer virus preparations were then used to infect Sf21 cells, which were harvested for membrane vesicle preparations.

Membrane Vesicle Preparation and Immunoblotting MRP1 Proteins. Membrane vesicles were prepared by nitrogen cavitation (*16*) and protein concentrations were determined by Bradford assay (Bio-Rad, Hercules, CA). ΔN-CL3 MRP1 and MRP1 CL3 internal deletion membrane proteins were subjected to SDS−7.5% PAGE and immunoblotted (*40*). MSD1 CL3-ΔC fragments along with $MRP1_{281-1531}$ were resolved on SDS−5−18% gradient polyacrylamide gels, while smaller CL3 fragments were analyzed on SDS−18% polyacrylamide gels. MRP1 was detected with either MAb QCRL-1 (*42*, *43*) and/or MAb MRPr1 (*44*, *45*), and β-gus was detected with rabbit anti-β-glucuronidase (Molecular Probes, Eugene, OR). Antibody−protein interactions were detected by horseradish peroxidase-conjugated secondary antibodies utilizing an enhanced chemiluminescence technique and subsequent exposure to film. Relative expression of MRP1 fragments was determined by densitometry.

For cell fractionation experiments, infected Sf21 cells were harvested and washed once with TB (50 mM Tris-HCl, pH 7.4, and 250 mM sucrose) and the cell pellet was snap-frozen at −70 °C. Crude membrane and cytosolic fractions were isolated as previously described (*6*). Briefly, cells were thawed on ice, swelled in TB buffer containing 10 mM KCl, 200 μg/mL EDTA, 1.5 mM $MgCl_2$, and Complete EDTA-free protease inhibitors for 10 min, and lysed with 80−100 stokes in a Tenbroeck homogenizer. The lysate was centrifuged at 900*g* and the pellet was discarded. Supernatant containing crude membranes and the cytosolic fraction was centrifuged at 100000*g* for 20 min at 4 °C. The supernatant (cytosolic fraction) was collected and the pellet (membrane fraction) was washed with TB and recentrifuged. Crude membranes were resuspended in TB by use of a 27.5 gauge needle. Proteins were quantified and detected as described above.

LTC_4 Transport into Sf21 Membrane Vesicles. Uptake of [^{3}H]-LTC_4 into membrane vesicles prepared from Sf21 cells has been described previously (*40*). Briefly, 4 μg of membrane vesicle protein was incubated with 50 nM LTC_4 in the presence of 4 mM ATP or AMP and 10 mM $MgCl_2$ in TB. Uptake was monitored over time, stopped by dilution in ice-cold TB, and filtered through glass fiber filters. Filters were washed twice with 4 mL of TB and bound radioactivity was determined by scintillation counting. ATP-dependent transport was determined by subtracting LTC_4 uptake in the presence of ATP from uptake in the presence of AMP.

Photoaffinity Labeling of MRP1 Constructs with [^{3}H]-LTC_4. Labeling of MRP fragments by [^{3}H]-LTC_4 was carried out as described previously (*32*). Briefly, Sf21 membrane vesicles (75 μg of protein) were incubated with 200 nM [^{3}H]-LTC_4 (0.25 μCi) in a final volume of 20 μL for 10 min at room temperature. Samples were frozen in liquid nitrogen and immediately UV-irradiated at 312 nm for 30 s and repeated 10 times. Tritium-labeled vesicle proteins were then resolved by SDS−PAGE before being subjected to fluorography.

Photoaffinity Labeling of MRP1 Constructs with [^{35}S]-Azidophenacyl-GSH. [^{35}S]-Azidophenacyl-GSH was synthesized as previously described (*38*, *46*, *47*). Briefly, 125 μCi of dithiothreitol- (DTT-) extracted [^{35}S]-GSH, 4-azidophenacylbromide (10 mM), GSH reductase (120 milliunits), and NADPH (1 mM) in 50 mM PBS (pH 7.4) was allowed to react for 1 h at room temperature. Reaction products were separated by Silica G thin-layer chromatography, and [^{35}S]-azidophenacyl-GSH was extracted. Photoaffinity labeling of MRP1 fragments was carried out as described previously (*38*). Briefly, vesicle protein (75 μg) was incubated with [^{35}S]-azidophenacyl-GSH at room temperature for 10 min and UV-irradiated for 5 min at 312 nm on ice. Labeled protein was run on an SDS−5−20% gradient polyacrylamide gel and subjected to fluorography.

Expression and Localization of MRP1 in MDCK-I Cells. Fugene6 was used to transfect cells with constructs cloned into the pCDNA 3.1(−) vector or pMG-H2 dual vector. Transfected cells were selected with Geneticin (800 μg/mL) or hygromycin (100 μg/mL) for 6−10 days. Stably transfected cell lines were maintained in antibiotic-supplemented medium. For localization of MRP1 proteins in MDCK-I cells, cells were seeded on glass coverslips and polycarbonate filters and grown for 2 weeks to allow polarization. Cells were fixed with cold 95% ethanol or 2% paraformaldehyde/1× PBS, pH 7.4 (10 min, RT); permeablized with 25 μg/mL digitonin/1× PBS, pH 7.4 (10 min, RT); and blocked with 1% bovine serum albumin (BSA)/1× PBS, pH 7.4 (block solution) (10 min, RT). Cells were then incubated with MRP1 MAb QCRL-3 (*42*) and/or MAb MRPr1 in block solution containing 1 μg/mL RNase A (1 h, RT) and subsequently washed once with block solution (10 min, RT). Alexa 488 and Alexa 546 goat anti-mouse and goat anti-rat secondary antibodies were used to detect protein−antibody interactions (1 h, RT). Cells were then washed twice with block solution (10 min, RT). In some cases, MRP1 antibodies were used in combination with either an anti-calnexin Mab or a polyclonal antiserum raised against canine Na^+/K^+-ATPase. Alexa 546 goat anti-rabbit or goat anti-chicken immunoglobins were used to detect antibody interactions with calnexin and Na^+/K^+-ATPase, respectively. Nuclei were stained either with propidium iodide, when only Alexa 488 secondary antibody was used, or with 7-aminoactinomycin D (7AAD), when cells were immunodetected with both Alexa 488 and Alexa 546 labeled secondary antibodies. The fluorescent secondary antibodies and nuclear stain were excited by use of a Leica TCS SP2 dual photon confocal microscope.

RESULTS

Identification of the NH_2-Proximal Functional Boundary of CL3. Figure 1A shows a topology of MRP1 generated by computer-assisted hydropathy analysis using the Eisenberg algorithm (*48*), which predicts that CL3 begins at amino acid 193 and ends at amino acid 301. On the basis of previous studies, the NH_2-proximal boundary of the functionally

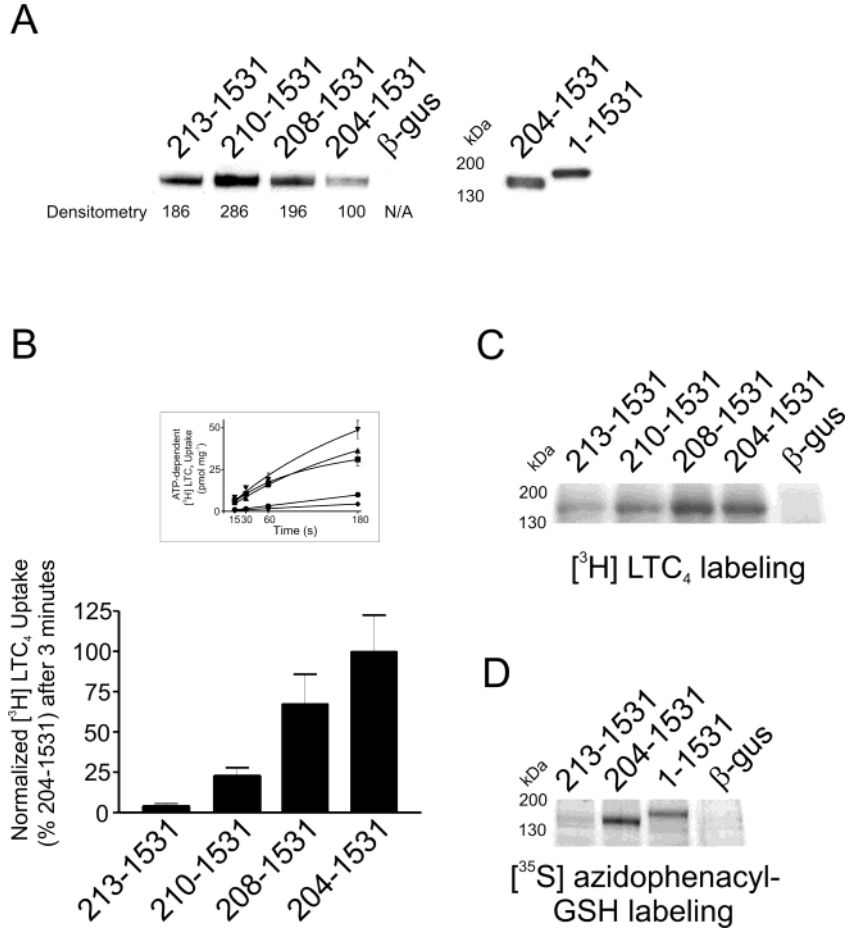

FIGURE 2: Characterization of ΔN-CL3 MRP1 construct LTC_4 transport and LTC_4 and azidophenacyl-GSH binding. (A) Immunoblot of wild-type MRP1 and ΔN-CL3 MRP1 constructs expressed in Sf21 insect cells detected with MAb QCRL-1. (B) Time course (inset) of ATP-dependent transport determined for $MRP1_{204-1531}$ (▲), $MRP1_{208-1531}$ (▼), $MRP1_{210-1531}$ (■), $MRP1_{213-1531}$ (●), and *β*-gus (◆). LTC_4 uptake observed for *β*-gus was subtracted from ΔN-CL3 MRP1 transport and rates were normalized for protein expression (shown in panel A) by densitometry. Fluorographs of MRP1 and ΔN-CL3 MRP1 labeled with (C) [^{3}H]-LTC_4 and (D) [^{35}S]azidophenacyl-GSH.

essential region of CL3 is predicted to lie between aa 204 and 227 (*30*, *33*). To define the boundary precisely, we generated finely spaced NH_2-proximal truncations between amino acids 204 and 213, referred to here collectively as ΔN-CL3 MRP1 (Figure 1B), and expressed these in insect Sf21 cells. Comparison of ΔN-CL3 MRP1 protein expression in Sf21 vesicles by densitometry showed that $MRP1_{208-1531}$, $MRP1_{210-1531}$, and $MRP1_{213-1531}$ were detected at 2.0-, 2.9-, and 1.9-fold higher levels, respectively, than $MRP1_{204-1531}$ (Figure 2A). LTC_4 uptake observed for $MRP1_{204-1531}$ was similar to that for wild-type MRP1 (not shown), as reported previously (*33*). After normalization to compensate for differences in protein expression levels and subtraction of control *β*-gus, the relative levels of ATP-dependent transport by $MRP1_{208-1531}$, $MRP1_{210-1531}$, and $MRP1_{213-1531}$ were 67%, 23%, and 4%, respectively, when compared to $MRP1_{204-1531}$ (Figure 2B).

To investigate whether decreased transport activity of the ΔN-CL3 MRP1 proteins reflected changes in their ability to bind substrate, we carried out photoaffinity labeling experiments using LTC_4. We have shown that removal of MSD1 by truncation to amino acid 204 does not affect LTC_4 binding compared to full-length MRP1 (*32*). Photolabeling of $MRP1_{208-1531}$ by [^{3}H]-LTC_4 was ~2-fold higher than observed for $MRP1_{204-1531}$, and after the differences in expression levels were taken into account, these proteins appeared to bind LTC_4 similarly. LTC_4 photolabeling of $MRP1_{210-1531}$ and $MRP1_{213-1531}$ was significantly decreased when compared to $MRP1_{208-1531}$ (Figure 2C), consistent with their reduced ability to transport LTC_4 being a consequence of impaired LTC_4 binding. Recently, we demonstrated that the GSH analogue azidophenacyl-GSH can substitute for GSH in enhancing the transport of estrone 3-sulfate and that the compound photolabels full-length MRP1 in a manner similar to that obtained with LTC_4 (*38*). The data illustrated in Figure 2D indicate that $MRP1_{204-1531}$ binds azidophenacyl-GSH as efficiently as wild-type MRP1 and that, like LTC_4, NH_2-proximal truncation to aa 213 severely impairs binding of the GSH analogue, as observed with LTC_4.

NH_2-Proximal Truncation of MRP1 to Amino Acid 210 Disrupts Plasma Membrane Localization in MDCK-I Cells. Mutated forms of ABC transporters, such as CFTR, that fail to traffic appropriately in mammalian cells and are rapidly degraded have been successfully expressed in insect cells where they are stable and active (*49*). To determine if the NH_2-proximal CL3 functional boundary identified by LTC_4 transport studies in insect cells also defined a region essential for the protein to traffic correctly in polarized cells, we prepared stable MDCK-I transfectants expressing the various ΔN-CL3 MRP1 mutants. It has been demonstrated that $MRP1_{204-1531}$, like the full-length protein, localizes to the basolateral membrane when expressed in a polarized mono-

layer of MDCK-II cells and that $MRP1_{281-1531}$ fails to traffic and accumulates in intracellular membranes (*31*, *33*). As observed previously, we found that $MRP1_{204-1531}$ localized to the cell-surface membranes of MDCK-I cells, as did $MRP1_{208-1531}$ (Figure 3 panels A,E and B,F). In contrast, $MRP1_{210-1531}$ and $MRP1_{213-1531}$ were both retained predominantly in cytoplasmic membranes (Figure 3 panels C,G and D,H). Furthermore, using markers for the basolateral membrane (Na^+/K^+-ATPase) (Figure 3A−D) and endoplasmic reticulum (calnexin) (Figure 3E−H), we found that $MRP1_{204-1531}$ and $MRP1_{208-1531}$ were detected primarily on basolateral membranes, while $MRP1_{210-1531}$ and $MRP1_{213-1531}$ were detected primarily in the endoplasmic reticulum (ER). Thus the decrease in LTC_4 transport activity and LTC_4 binding observed when these constructs were expressed in insect cells is also associated with impaired trafficking in MDCK-I cells.

Identification of the COOH-Proximal Functional Boundary of CL3. We have shown that the coexpression of $MRP1_{1-281}$ with two inactive NH_2-terminal truncated polypeptides, $MRP1_{281-1531}$ or $MRP1_{229-1531}$, restores the ability to transport and bind LTC_4, while coexpression of $MRP1_{1-227}$ with $MRP1_{229-1531}$ does not (*30*). This suggests that the physical integrity of a region between amino acids 204−280, spanning amino acids 227−229, is important for MRP1 transport activity. To define the CL3 functional boundary between aa 229 and 280, constructs were engineered to truncate the COOH-proximal end of $MRP1_{1-281}$. Fragments were created terminating at amino acids 255, 260, 270, and 280, referred to collectively as MSD1-CL3 ΔC (Figure 1C). These NH_2-proximal fragments were then coexpressed in Sf21 cells with $MRP1_{281-1531}$. Similar expression levels of the various MSD1-CL3 ΔC fragments and $MRP1_{281-1531}$ were obtained in the pFastBac DUAL expression vector. The only exception was $MRP1_{1-280}$, which for unknown reasons was expressed at levels somewhat lower than the other fragments (Figure 4A). Transport studies showed that $MRP1_{1-280}$ (22 ± 3 pmol mg^{-1} after 3 min) and $MRP1_{1-260}$ (23 ± 2 pmol mg^{-1} after 3 min) both restored LTC_4 uptake when expressed with $MRP1_{281-1531}$, while $MRP1_{1-255}$ did not increase transport (3 ± 1 pmol mg^{-1} after 3 min) (Figure 4B) above that observed for the large fragment alone (not shown). Similarly, the ability to photolabel $MRP1_{281-1531}$ with LTC_4 (Figure 4C) or azidophenacyl-GSH (Figure 4D) was low upon coexpression with $MRP1_{1-255}$ compared with coexpression with $MRP1_{1-260}$. As reported previously (*38*), the MSD1-CL3 ΔC fragments themselves were not photolabeled with LTC_4 (not shown) or azidophenacyl-GSH (Figure 4D).

To further define the COOH-proximal functional boundary of CL3, additional MSD1-CL3 ΔC constructs were generated between aa 255 and 260. These were coexpressed with $MRP1_{281-1531}$ (Figure 4E) and analyzed for the ability to reconstitute LTC_4 transport (Figure 4F). After vesicle uptake was normalized to protein levels of the common, larger MRP1 fragment, $MRP1_{1-259}$ and $MRP1_{1-257}$ were able to reconstitute 75% and 43% of LTC_4 transport activity, respectively, when compared to uptake observed in the presence of $MRP1_{1-260}$. $MRP1_{1-256}$ did not reconstitute LTC_4 transport to a level that was demonstrably higher than that observed for $MRP1_{1-255}$ (Figure 4F).

CL3 Amino Acids 261−280 Are Important for Plasma Membrane Targeting in MDCK-I Cells. The NH_2-proximal functional boundary defined by LTC_4 transport in Sf21 cells coincided with the boundary of the region in CL3 required for membrane localization in MDCK-I cells. To determine whether this was also true of the COOH-proximal boundary, MSD1-CL3 ΔC proteins were expressed with $MRP1_{281-1531}$ in MDCK-I cells via the pMG-H2 mammalian dual-expression vector. MSD1-CL3 ΔC and $MRP1_{281-1531}$ proteins could be detected in the same cells by use of MAb MRPr1 and MAb QCRL-3, respectively, with appropriate red and green fluorescent secondary antibodies. However, we found that MRPr1 staining was weak when cells were fixed with paraformaldehyde, while immunofluorescent detection of QCRL-3 was lower after ethanol fixation. Consequently, immunofluorescence studies were carried out with both fixation protocols. $MRP1_{1-255}$ (not shown) and $MRP1_{1-260}$ (red signal) when dual-expressed with $MRP1_{281-1531}$ (green signal) were unable to rescue trafficking of the larger MRP1 fragment (Figure 5, left panels). $MRP1_{281-1531}$ was detected predominantly in intracellular membranes (Figure 5, upper left panel), possibly the endoplasmic reticulum since when expressed alone this fragment colocalized with calnexin (not shown). However, $MRP1_{1-255}$ (not shown) and $MRP1_{1-260}$ were detected predominately in large intracellular bodies that did not colocalize with the ER-like staining observed for the remainder of the protein (Figure 5, middle and lower left panels). Previous studies have reported that $MRP1_{1-280}$ expressed alone in MDCK-II cells was detected in large intracellular vesicles rather than on the plasma membrane (*33*). We observed similar results after transient expression of $MRP1_{1-255}$, $MRP1_{1-260}$, $MRP1_{1-270}$, and $MRP1_{1-280}$ in ethanol-fixed MDCK-I cells (not shown). When $MRP1_{1-280}$ was coexpressed with $MRP1_{281-1531}$, both fragments were detected on basolateral membranes in MDCK-I cells (not shown). Similarly, MRP_{1-270} rescued the basolateral trafficking of the larger coexpressed MRP1 fragment (Figure 5, right panels), although slightly less efficiently than observed in the presence of $MRP1_{1-280}$. Vertical sections through the monolayer of cells expressing MSD1-CL3 ΔC fragments and the remainder of MRP1 showed that rescued $MRP1_{281-1531}$ and $MRP1_{1-270}$ were concentrated in or near the basolateral membranes between adjacent cells (Figure 5, lower right panel). Thus, although $MRP1_{1-260}$, like $MRP1_{1-280}$ and $MRP1_{1-270}$, rescued the function of $MRP1_{281-1531}$ in insect cells, it failed to support correct trafficking in polarized MDCK-I cells. Furthermore, $MRP1_{1-260}$ and $MRP1_{281-1531}$ did not colocalize when coexpressed.

$MRP1_{204-270}$ Expressed with $MRP1_{281-1531}$ Reconstitutes LTC_4 Uptake and Binding. Although CL3 is predicted by most topology programs to be cytoplasmic, a fragment comprised of aa 204−280 appears to associate with cellular membranes independently of the presence of a MSD or predicted TM helix (*31*). In addition, $MRP1_{204-280}$ has been reported to reconstitute the LTC_4 transport activity of $MRP1_{281-1531}$ and partially restore this fragment's localization to basolateral membranes in MDCK-II cells (*31*). To explore the possibility that the presence of MSD1 might influence the location of the COOH-proximal functional boundary of CL3, we repeated the studies above with $MRP1_{204-280}$, $MRP1_{204-270}$, and $MRP1_{204-260}$ (Figure 1D). Analysis of membrane vesicle proteins by immunoblotting showed that $MRP1_{204-270}$ and $MRP1_{204-280}$ were present at similar levels.

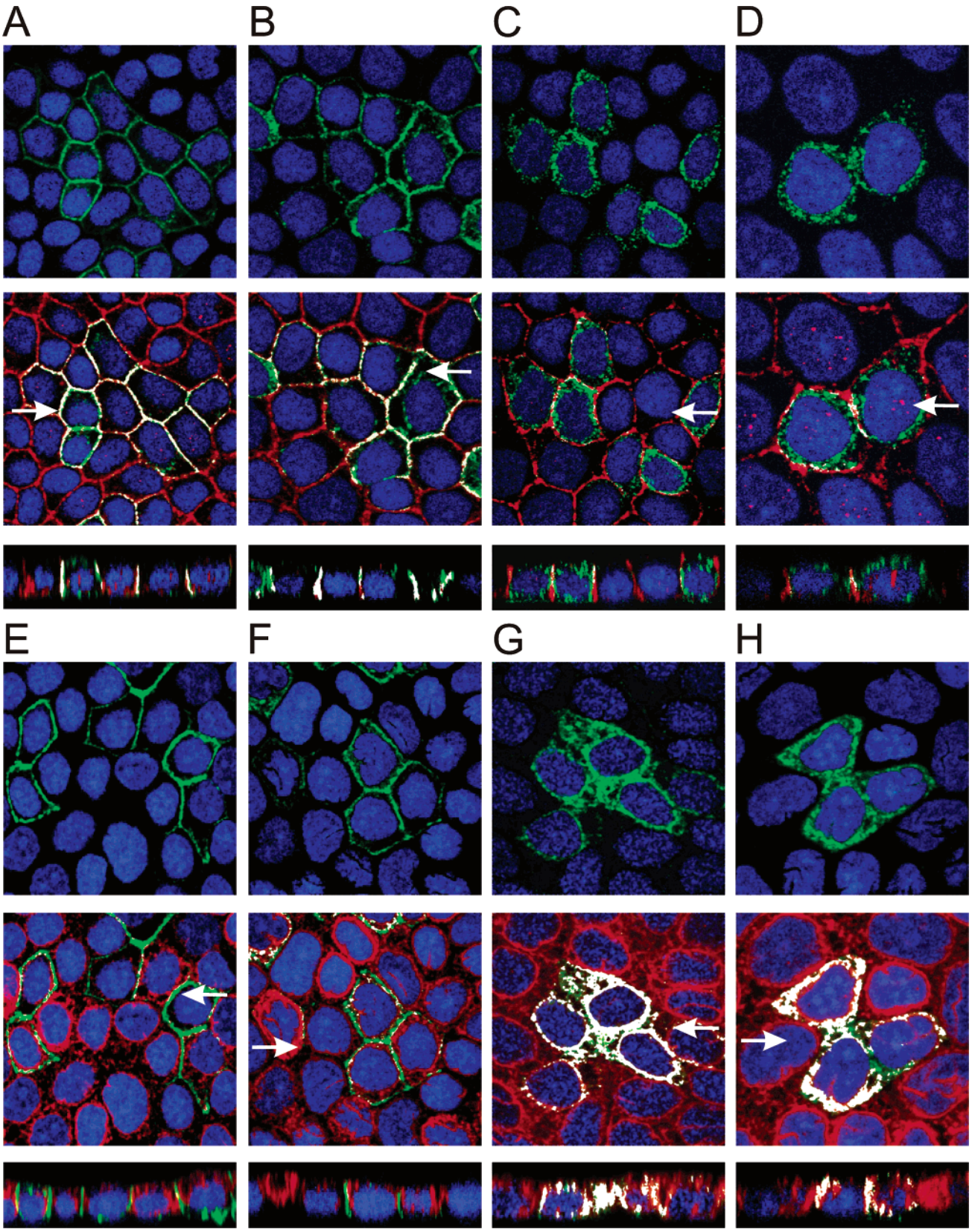

FIGURE 3: Colocalization of ΔN-CL3 MRP1 constructs with cellular markers in MDCK-I cells. $MRP1_{204-1531}$ (A and E), $MRP1_{208-1531}$ (B and F), $MRP1_{210-1531}$ (C and G), and $MRP1_{213-1531}$ (D and H) stably expressed in MDCK-I cells were detected by indirect immunofluorescence by use of confocal scanning microscopy after ethanol fixation with MAb MRPr1 and goat anti-rat Alexa 488 (green). Middle panels show overlay of cells in the top panels stained with either the basolateral membrane marker Na^+/K-ATPase polyclonal antibody immunodetected with goat anti-chicken Alexa 546 (A−D; red) or the endoplasmic reticulum marker MAb anti-calnexin detected with goat anti-rabbit Alexa 546 (E−H; red). Nuclei were counterstained with 7-AAD (blue). White arrows mark the position of the vertical *x*/*z* sections made through the cells shown in the lower panels. White areas in triple-stained images indicate areas of colocalization of the cellular protein marker with ΔN-CL3 MRP1 proteins.

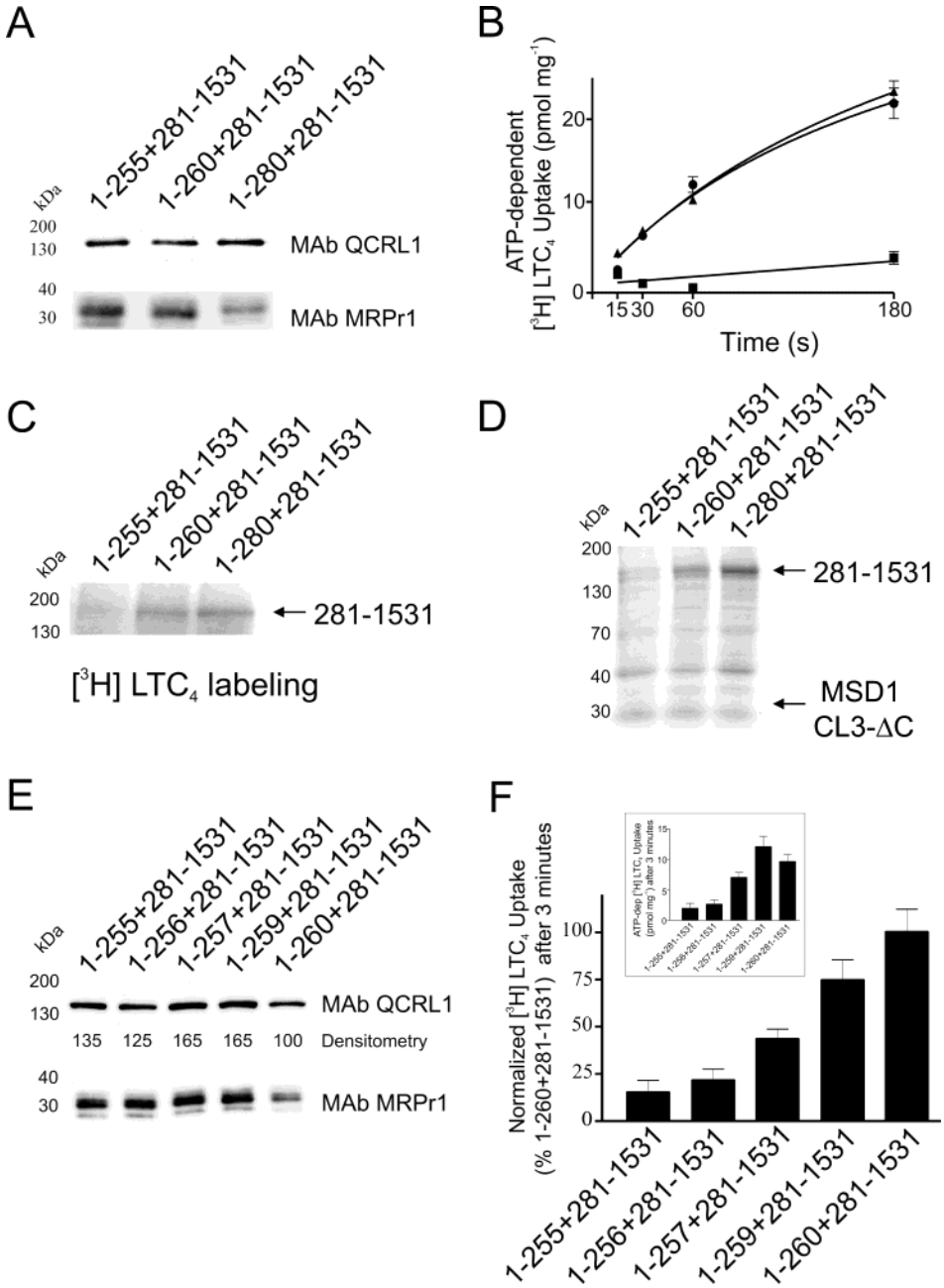

FIGURE 4: Characterization of MSD1 CL3-ΔC reconstitution of $MRP1_{281-1531}$ LTC_4 transport and LTC_4 and azidophenacyl-GSH binding. (A, E) Immunoblot of MSD1 CL3-ΔC fragments dual-expressed with $MRP1_{281-1531}$ (4 μg of vesicle protein/lane) in the pFastBac DUAL system. MAb QCRL-1 (upper panel) and MAb MRPr1 (lower panel) were used to detect MRP1 fragments. (B) ATP-dependent LTC_4 transport observed for dual-expressed MRP1 fragments: $MRP1_{1-280}$ + $MRP1_{281-1531}$ (▲), $MRP1_{1-260}$ + $MRP1_{281-1531}$ (●), and $MRP1_{1-255}$ + $MRP1_{281-1531}$ (■). (C, D) Fluorographs of [^{3}H]-LTC_4- (C) and [^{35}S]-azidophenacyl-GSH- (D) labeled $MRP1_{281-1531}$ dual-expressed with MSD1-CL3 ΔC fragments. (F) ATP-dependent LTC_4 uptake observed for dual-expressed MRP1 fragments. Transport rates (inset) were normalized for $MRP1_{281-1531}$ expression in panel E by densitometry.

However, very little $MRP1_{204-260}$ could be detected (Figure 6A). ATP-dependent LTC_4 uptake for $MRP1_{204-270}$ or $MRP1_{204-280}$ coexpressed with $MRP1_{281-1531}$ was 27 ± 2 and 38 ± 2 pmol mg^{-1}, respectively, after vesicles were incubated with substrate for 3 min, while only 5 ± 1 pmol mg^{-1} of transport activity was observed after the same time period in vesicles coexpressing $MRP1_{204-260}$ and $MRP1_{281-1531}$ (Figure 6B). As expected from the transport assays, coexpression of $MRP1_{204-270}$ with $MRP1_{281-1531}$ restored LTC_4 labeling of the larger MRP1 fragment (Figure 6C).

To explain the apparently low levels of $MRP1_{204-260}$, we considered the possibility that its immunodetection may have been diminished because of the proximity of the MRPr1 epitope (amino acids 238−247) to the COOH-terminus of this fragment (*44*). However, this appears unlikely given that no difficulty was encountered detecting $MRP1_{1-260}$ (Figure 4A). As an alternative, we investigated whether removal of amino acids 260−269 had abolished plasma membrane association. To determine if plasma membrane association was disrupted, CL3 peptides were coexpressed with the cytosolic protein β-gus, and their subcellular localization was compared in Sf21 cells. The CL3 peptides were almost entirely detected in crude membranes including $MRP1_{204-260}$, while, as expected, β-gus was found mainly in the cytosolic fractions (Figure 6D). Although $MRP1_{204-260}$ appeared to associate with membranes, expression levels of the peptide

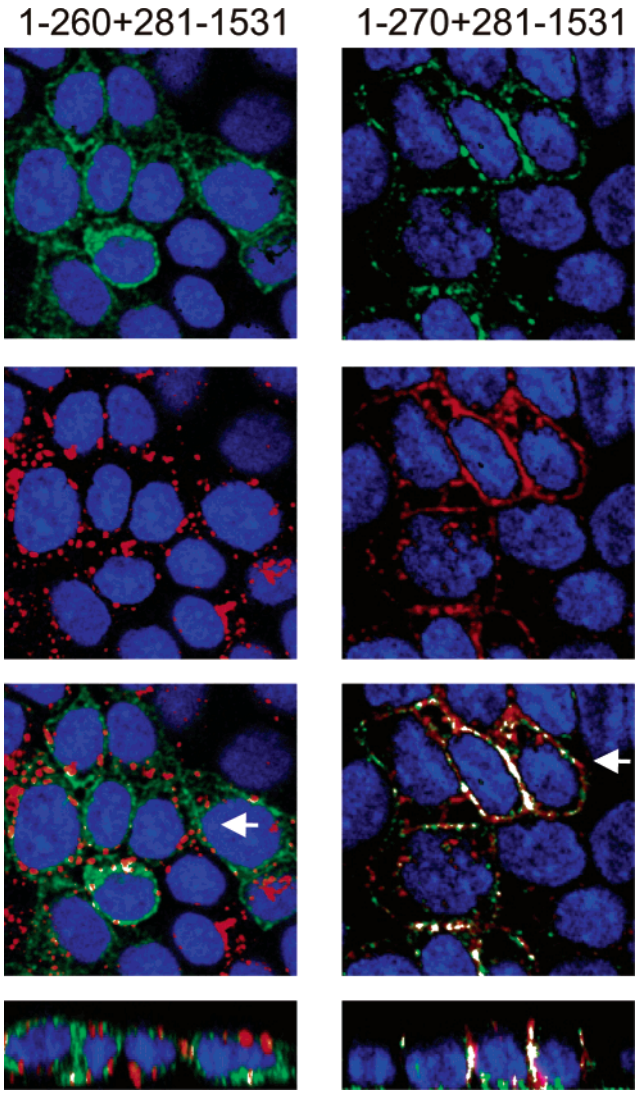

FIGURE 5: Reconstitution of basolateral trafficking of $MRP1_{281-1531}$ by MSD1-CL3 ΔC fragments in MDCK-I cells. MSD1-CL3 ΔC fragments $MRP1_{1-260}$ and $MRP1_{1-270}$ were dual-expressed with $MRP1_{281-1531}$ in MDCK-I cells with the pMG-H2 vector. Polarized cells were fixed in 95% ethanol and MSD1-CL3 ΔC fragments were detected with MAb MRPr1 and goat anti-rat Alexa 546 (red), while $MRP1_{281-1531}$ was immunostained with MAb QCRL-3 and goat anti-mouse Alexa 488 (green). White arrows in the triple-stained overlays denote the position of the vertical *x*/*z* section through the cells shown in the lower panels. White areas indicate areas of colocalization of the coexpressed MRP1 fragments. Nuclei were counterstained with 7-AAD (blue).

determined by immunoblotting with MAb MRPr-1 were consistently 10−20-fold lower than observed for other CL3 peptides, suggesting a possible problem in the folding and maturation of the fragment and its rapid degradation.

A COOH-Proximal Internal Deletion in CL3 Does Not Affect Transport in Insect Vesicles but Impairs Trafficking in MDCK-I Cells. Previously, it has been shown that internal deletion of CL3 residues 223−232 rendered MRP1 inactive for LTC_4 transport (*31*). Despite its lack of activity, this mutant appeared to traffic normally to the basolateral membranes of MDCK-II cells (*31*). The MSD1-CL3 ΔC fragment ending at Asp^{260} displayed the opposite behavior. It was able to reconstitute transport of $MRP1_{281-1531}$ in Sf21 cells but failed to rescue trafficking in MDCK-I cells. Consequently, we also ascertained the effects of deleting amino acids 261−279 in the intact protein (Figure 1F). Densitometry of immunoblots of Sf21 vesicles showed that MRP1 Δ(261−279) and MRP1 Δ(271−279) were expressed at 2.3- and 1.5-fold higher levels, respectively, than wild type (Figure 7A). ATP-dependent uptake observed for the wild-type protein and CL3 internal deletions were similar after subtraction of control β-gus transport and normalization for relative protein expression levels (Figure 7B). Thus the protein is able to adopt an active conformation in insect cells despite the possible topographical distortion introduced by internal deletion of 19 amino acids from CL3. In addition, internal deletion of amino acids 271−279 had little effect on basolateral localization compared with wild-type MRP1 in polarized MDCK-I cells, as evident by colocalization with the basolateral membrane marker (Figure 7C, left and center panels). In contrast, deletion of amino acids 261−279 resulted in most of the mutant protein being localized in membranes surrounding large vesicles, with only a minor fraction being detected on or near the basolateral membrane (Figure 7C, right panels). Thus the results obtained with these internal deletion mutants support data from coexpression studies indicating that amino acids 261−269 are critical for trafficking but not for the protein to adopt a functional configuration in insect cells.

DISCUSSION

Several lines of evidence indicate that the region of CL3 between amino acids 204 and 280 is essential for substrate binding, as well as appropriate trafficking of MRP1 in mammalian cells. This region also appears to be capable of forming stable interactions with the remainder of the protein based on its ability to rescue the trafficking of an MRP1 fragment truncated to amino acid 281. A number of secondary structure algorithms predict that the region of CL3 between amino acids 204 and 280 contains two helical motifs (Figure 8A). Previous reports have speculated that a helix predicted to be located between amino acids 221 and 233 is required for membrane association and MRP1 function (*31*). The secondary structure predicted by the program PhD Predict is most similar to that proposed previously, while most programs predict that the NH_2-proximal helical region of CL3 begins between amino acids 211 and 216 and ends with a highly conserved glycine at position 231 (Figure 8A). These analyses also identified a second helical element between amino acids 247 and 267, the secondary structure of which appears to be conserved among evolutionarily diverse ABCC family members from *Saccharomyces cerevisiae*, *Caenorhabditis elegans*, and plants (Figure 8A).

We have now defined the boundaries of the region in CL3 that are required for substrate binding and transport in Sf21 insect cells and determined whether they coincide with the boundaries of the region required for correct protein folding and efficient trafficking in polarized mammalian cells. Insect cells are able to express mutant proteins that are recognized as misfolded and are retained and degraded in the endoplasmic reticulum of mammalian cells. This may be due to differences in the stringency of the protein processing machinery. Alternatively, the lower growth temperatures (28 °C) typically used for growing insect cells may reduce the free energy requirements for protein folding (*49*). These differences between insect and mammalian cells offer the opportunity to distinguish between regions of a protein that

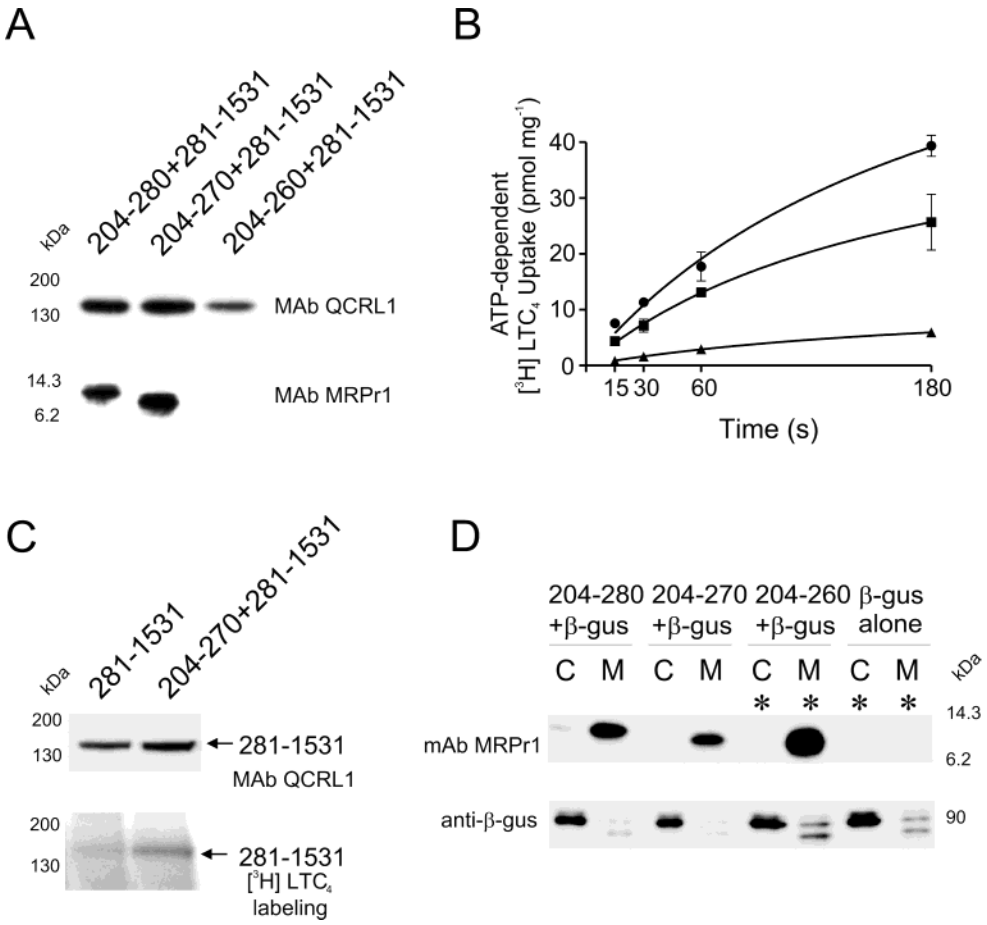

FIGURE 6: CL3-mediated LTC_4 transport reconstitution and plasma membrane association. (A) Immunoblot of MRP1 CL3 fragments, resolved on an SDS−18% polyacrylamide gel (lower panel), coexpressed with $MRP1_{281-1531}$, separated on an SDS−7.5% polyacrylamide gel (upper panel), in the pFastBac expression system. (B) ATP-dependent LTC_4 transport was measured for coexpressed $MRP1_{204-280}$ + $MRP1_{281-1531}$ (●), $MRP1_{204-270}$ + $MRP1_{281-1531}$ (■), and $MRP1_{204-260}$ + $MRP1_{281-1531}$ (▲). (C) Immunoblot (upper panel) of $MRP1_{281-1531}$ fragment detected with MAb MRPr-1 expressed alone and dual-expressed with $MRP1_{204-270}$ in the pFastBac DUAL vector, and fluorograph (lower panel) of [^{3}H]-LTC_4-labeled $MRP1_{281-1531}$. (D) Detection of dual-expressed CL3 fragments (SDS−18% PAGE, MAb MRPr1, upper panel) and β-gus (SDS−10% PAGE, anti-β-gus, lower panel) in cytoplasmic fractions (lanes marked C) and membrane fractions (lanes marked M). To immunodetect approximately equivalent molar amounts of the CL3 fragments, lanes marked with asterisks in the CL3 MAb MRPr-1 immunoblot had 20 μg of protein loaded, while all others contained 1 μg of protein/lane. Samples run on the anti-β-gus immunoblot had 1 μg of protein/lane.

are intrinsically important for function, as opposed to regions that are required for efficient maturation and trafficking.

In Sf21 cells, NH_2-proximal truncations of MRP1 to Cys^{208}, Glu^{210}, and Ala^{213} decreased LTC_4 transport by approximately 30%, 75%, and more than 90%, respectively, relative to $MRP1_{204-151}$ (Figure 2B). These analyses indicate that the NH_2-terminal boundary of the essential region of CL3 is located at the beginning of the predicted helix between aa 211 and 231. Photolabeling studies demonstrate that inefficient transport by NH_2-proximal CL3 truncations is associated with a reduced ability to bind LTC_4 (Figure 2C). Parallel studies with the photoactivable GSH analogue azidophenacyl-GSH also demonstrated that MSD1 is not required for glutathione binding, while CL3 residues between amino acids 204 and 213 are essential (Figure 2D). Furthermore, in polarized MDCK-I cells, trafficking of $MRP1_{208-1531}$ was comparable to that of $MRP1_{204-1531}$, while that of $MRP1_{210-1531}$ and $MRP1_{213-1531}$ was severely impaired and both truncated proteins colocalized with the ER chaperone calnexin (Figure 3). These data suggest that removal of Cys^{208} and Pro^{209} impairs the maturation and sorting of the mutant protein in the ER, resulting in rapid degradation. This is supported by studies in which we have shown that the steady-state levels of $MRP1_{210-1531}$ and $MRP1_{213-1531}$ in membrane vesicles of stably transfected HEK293 cells were less than 10% of those obtained with $MRP1_{204-1531}$ (not shown).

Among the ABCC proteins, the identity of amino acids corresponding to MRP1 Cys^{208} is not highly conserved, although all residues found at the corresponding positions are polar (Figure 8A). In contrast, Pro^{209} is highly conserved among MRP1-related proteins. On the basis of the data obtained, it is possible that amino acids 208 and 209 could be involved directly in substrate binding or alternatively could be required for correct folding of the protein. However, this seems unlikely since, we have recently found that alanine substitution at either of these positions did not affect MRP1 expression or transport activity in stably transfected HeLa cells (*50*, *51*). Alternatively, it is possible that in the absence of MSD1, removal of Cys^{208} and Pro^{209} may affect the structural integrity of CL3 by decreasing the stability of the NH_2-proximal part of helix 1. The TMHMM algorithm (*52*) identified helix 1 in CL3 as a low probability (20%) TM helix and predicts that truncation of $MRP1_{204-1531}$ to Glu^{210} or Ala^{213} would decrease the probability of a helix forming

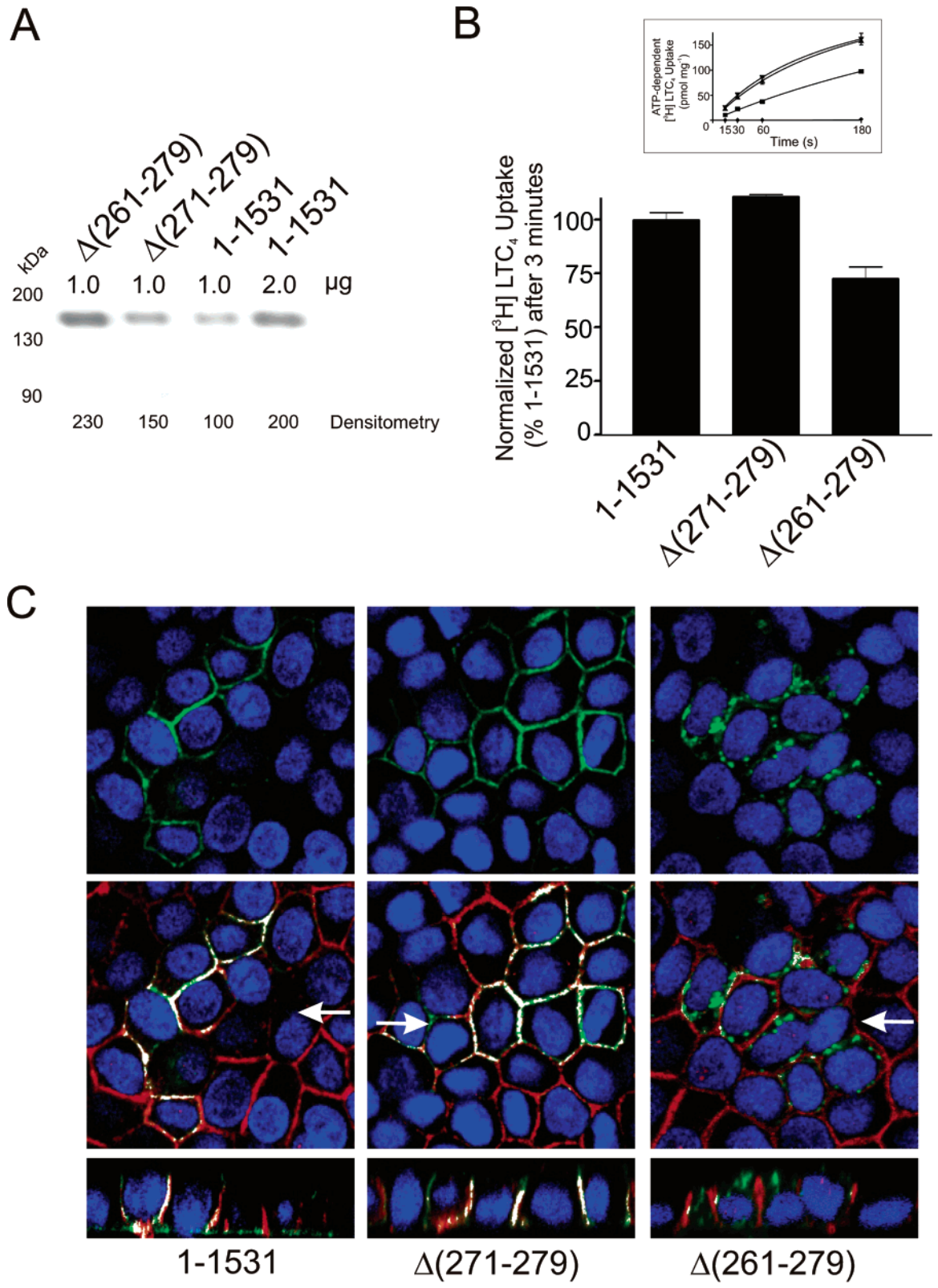

FIGURE 7: LTC_4 transport and membrane trafficking of MRP1 CL3 internal deletions. (A) Immunoblot of wild-type and CL3 internal deletion proteins expressed in Sf21 membrane vesicles (1 μg/lane) immunodetected with MAb QCRL-1. (B) Time course (inset) of ATP-dependent LTC_4 transport in Sf21 membrane vesicles for MRP1 (1−1531) (■), MRP1 Δ(271−279) (▲), and MRP1 Δ(261−279) (▼). Uptake was normalized for protein expression by densitometry (A) and control β-gus was subtracted. (C) Indirect immunofluorescence of wild-type and MRP1 CL3 internal deletion constructs stably expressed in polarized MDCK-I cells grown on polycarbonate filters. Cells were fixed with ethanol and immunodetected with MAb MRPr1 and goat anti-rat Alexa 488 (green) and the Na^+/K-ATPase polyclonal antibody and goat anti-chicken Alexa 546 (red). Arrows indicate the position of the vertical *x*/*z* section (lower panels) through the monolayer. White areas indicate areas of colocalization of the basolateral membrane marker and MRP1 proteins. Nuclei were counterstained with 7-AAD (blue).

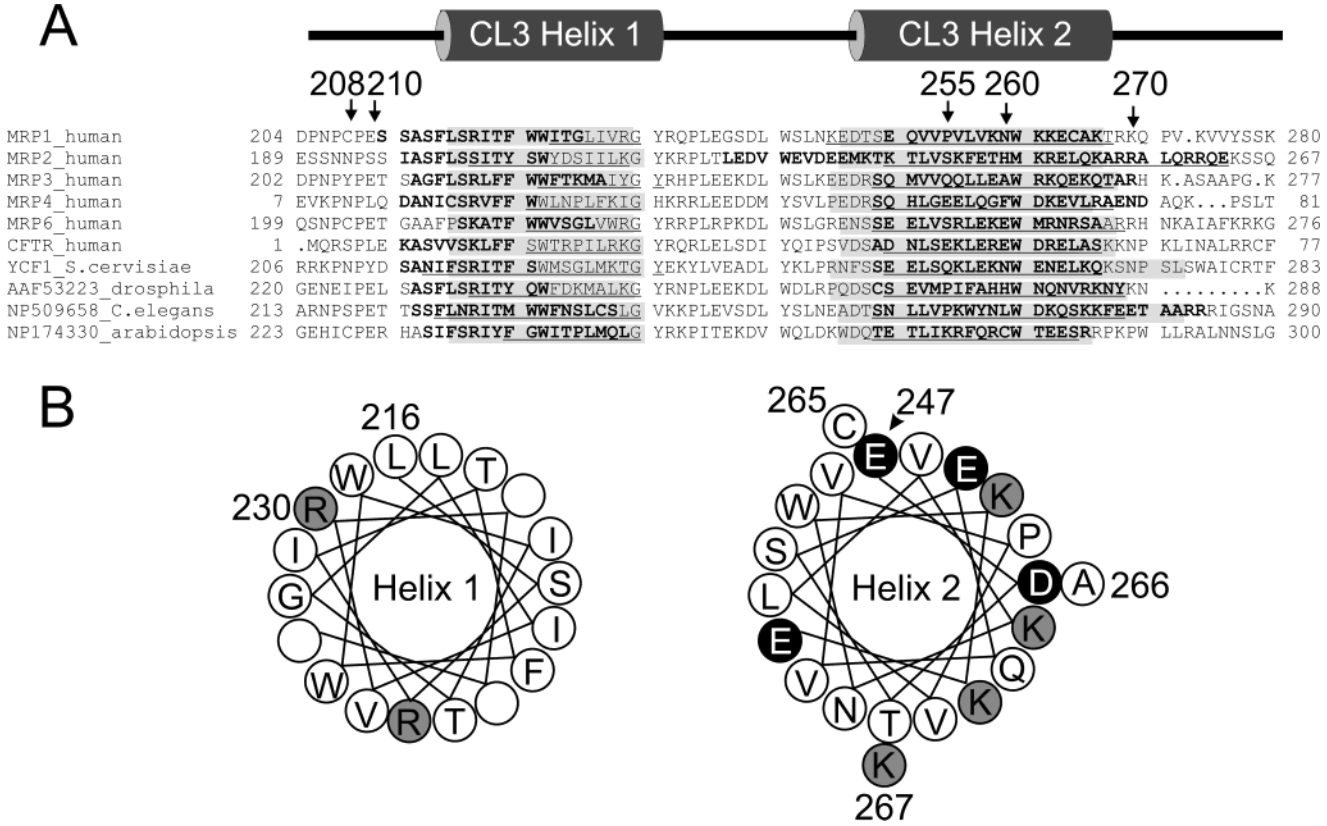

FIGURE 8: Secondary structure prediction of CL3. (A) Alignment of MRP1 CL3 with the corresponding cytoplasmic regions of related proteins. Computer-assisted secondary structure prediction algorithms [highlighted residues, PSIpred (*62*); boldface residues, SOMPA (*63*); underlined residues, PhD (*64*)] were used to identify structural elements within the aligned sequences. (B) Helical wheel projection of PSIpred-predicted CL3 helices. Shaded circles indicate charged residues.

at this location to below 5%. Studies of the topology of MRP1 essentially preclude the possibility that helix 1 in CL3 traverses the membrane. However, the NH_2-terminal region of the recently crystallized bacterial vitamin D transporter subunit, BtuC, contains a TM helix (residues 2−32) that appears to be laterally associated with or embedded in the inner leaflet of the lipid bilayer (*53*). Although there is no discernible primary structure homology between this region of BtuC and CL3 in MRP1, when the region between amino acids 204 and 260 is expressed independently of the remainder of the protein, it can be recovered predominantly associated with membranes (Figure 6D). Thus the ability of the NH_2-proximal helical region of CL3 to interact with the membrane in a manner analogous to that observed in BtuC may be a requirement for correct folding and trafficking of the protein.

COOH-proximal truncation of $MRP1_{1-280}$ to Asn^{260} did not affect the ability of this fragment to rescue LTC_4 and azidophenacyl-GSH binding and LTC_4 transport when expressed with $MRP1_{281-1531}$ in Sf21 cells (Figure 4B,C). Recently, it has been suggested that Trp^{261} and Lys^{267} form part of a binding site for 11-azidoagosterol A (*34*). While regions of CL3 appear essential for binding of substrate, most studies with photoactivatable substrates (LTC_4), inhibitors (AG-A, LY475776), and GSH derivatives (azidophenacyl-GSH) have failed to detect cross-linking to sites in CL3 (*32*, *34*, *38*). The exception is a recent study with the GSH analogue arylazido-GSH (IAAGSH), in which very weak labeling of a tryptic fragment believed to correspond to CL3 was reported (*54*). However, the stoichiometry of labeling of CL3 compared with predominantly labeled sites in MSD2 and MSD3 is not known. Studies on the sulfonylurea receptor SUR1 (ABCC8) also indicate that regions of CL3 are necessary for the binding of glibenclamide, but as with most studies of MRP1, direct photolabeling of these regions has not been demonstrated (*55*). Taken together with earlier photolabeling studies with gliburide analogues, these studies suggest that MSD1 of SUR1 interacts directly with the ligand rather than MSD2 and MSD3 as found during studies of MRP1 (*56*).

Further COOH-proximal truncation of $MRP1_{1-260}$ to Lys^{259} and Leu^{257}caused a 25% and 75% reduction in its ability to reconstitute LTC_4 transport, respectively, while fragments ending at Val^{256} or Pro^{255} completely failed to stimulate transport in the presence of $MRP1_{281-1531}$ (Figure 4B,F). Substrate photolabeling studies indicated that $MRP1_{1-255}$ failed to restore LTC_4 and azidophenacyl-GSH binding by the larger MRP1 fragment (Figure 4C,D). Truncation to Pro^{255} eliminates the hydrophobic tripeptide Val^{256}-Leu^{257}-Val^{258} and is predicted to disrupt the COOH-proximal helix of CL3. Thus the COOH-proximal boundary is within helix 2 near a cluster of hydrophobic amino acids predicted to be critical for maintaining stability of the remainder of the helix. Complete loss of the COOH-proximal helix of CL3 may eliminate the ability of the fragment to interact with the remainder of the protein. Whereas the NH_2-proximal functional and trafficking boundaries of CL3 coincide, the locations of the COOH-proximal boundaries differ. The

region between amino acids 261 and 269 is not required for function in insect cells but it is necessary for trafficking and appropriate membrane localization in MDCK-I cells. Dual expression of $MRP1_{1-270}$ was only slightly less effective than $MRP1_{1-280}$ (not shown) at restoring trafficking of the MRP1 core to the basolateral plasma membrane, while $MRP1_{1-260}$ was completely ineffective, consistent with a loss of interaction between the two fragments (Figure 5). In support of this suggestion, the immunofluorescent signal observed for $MRP1_{1-260}$ was found in large intracellular bodies, potentially in vesicles of the Golgi apparatus and/or endosomes or undergoing degradation by the proteosome, while the core was observed in distinctly different regions of the cell, likely the ER (Figure 5, left panels). Recently, it has been reported that MRP1 MSD1 lacking all of CL3, could be detected at the cell surface when expressed in *Xenopus* oocytes, although what percentage of the fragment remained cytoplasmic was not assessed (*57*). At present, it is not known whether this might be attributable to differences in protein processing between *Xenopus* oocytes and the mammalian cell lines used here. However, it appears possible that the presence of parts of CL3 in the NH_2-terminal fragments we have used impairs the ability of MSD1 to traffic to or be retained in the plasma membrane in the absence of the MRP1 core. We have also established that amino acids 260−269 are not simply required for membrane association. Although the peptide comprising amino acids 204−260 failed to rescue transport of $MRP1_{281-1531}$ and was expressed at relatively low levels, it was nevertheless recovered exclusively in a membrane-associated fraction (Figure 6A,B,D). Similarly, internal deletion of Trp^{261}−Ser^{279} from full-length MRP1 had no effect on LTC_4 transport activity in insect cells (Figure 7B) but caused significant defects in basolateral membrane trafficking (Figure 7C, right panels) and resulted in accumulation of the mutant protein in large vesicles, similar to the distribution observed for $MRP1_{1-260}$. In contrast, deletion of Gln^{271}−Ser^{279} had no effect on trafficking. Since amino acids 260−267 comprise the COOH-proximal half of helix 2, the structural integrity of this domain may be required for correct protein folding and/or trafficking in mammalian cells (Figure 8A).

The nature of the interactions between the critical region of CL3 and the remainder of the protein is not yet known. Recent reports have suggested that CFTR contains an α-helix between Ala^{46} and Ser^{63} (*58*). This location aligns with MRP1 CL3 helix 2 (Figure 8A), and it has been proposed that acidic residues in this helical region of CFTR contribute to regulation of channel activity by interacting with the regulatory R domain of the protein (*58*, *59*). In addition, syntaxin 1A has been shown to interact with the NH_2-terminal region of CFTR, which aligns with MRP1 CL3, and to potentially regulate trafficking of the protein to and from cellular membranes (*60*, *61*). One unusual feature of the region of CL3 containing helix 2 is its exceptionally high content of charged amino acids. There are a total of 13 positively charged and four negatively charged residues in the region bounded by Lys^{246} and Lys^{280}. Helical wheel projections show that ∼40% of the amino acids in helix 2 are charged (Figure 8B), as are 6 of 10 residues between Trp^{261} and Lys^{270}, a region that is critical for proper folding and trafficking of the protein in MDCK-I cells but not for transport activity in Sf21 cells. Whether the charged residues contribute ionic linkages with other parts of MRP1 that promote proper protein folding and trafficking or are involved in interactions with other proteins important for appropriate trafficking of MRP1 is currently under investigation.

ACKNOWLEDGMENT

We thank Derek Schulze for expert advice on confocal microscopy.

REFERENCES

1. Ambudkar, S. V., Dey, S., Hrycyna, C. A., Ramachandra, M., Pastan, I., and Gottesman, M. M. (1999) Biochemical, cellular, and pharmacological aspects of the multidrug transporter, *Annu. Rev. Pharmacol. Toxicol. 39*, 361−398.
2. Cole, S. P., Bhardwaj, G., Gerlach, J. H., Mackie, J. E., Grant, C. E., Almquist, K. C., Stewart, A. J., Kurz, E. U., Duncan, A. M., and Deeley, R. G. (1992) Overexpression of a transporter gene in a multidrug-resistant human lung cancer cell line, *Science 258*, 1650−1654.
3. Deeley, R. G., and Cole, S. P. (2003) Multidrug Resistance Protein 1 (ABCC1), in *ABC Proteins: From Bacteria to Man* (Holland, I. B., Ed.) pp 393−422, Elsevier Science, New York.
4. Bates, S. E. (2003) Solving the Problem of Multidrug Resistance: ABC Transporters in Clinical Oncology, in *ABC Proteins: From Bacteria to Man* (Holland, I. B., Ed.) pp 359−391, Elsevier Science, New York.
5. Cole, S. P., Sparks, K. E., Fraser, K., Loe, D. W., Grant, C. E., Wilson, G. M., and Deeley, R. G. (1994) Pharmacological characterization of multidrug resistant MRP-transfected human tumor cells, *Cancer Res. 54*, 5902−5910.
6. Grant, C. E., Valdimarsson, G., Hipfner, D. R., Almquist, K. C., Cole, S. P., and Deeley, R. G. (1994) Overexpression of multidrug resistance-associated protein (MRP) increases resistance to natural product drugs, *Cancer Res. 54*, 357−361.
7. Leier, I., Jedlitschky, G., Buchholz, U., and Keppler, D. (1994) Characterization of the ATP-dependent leukotriene C_4 export carrier in mastocytoma cells, *Eur. J Biochem. 220*, 599−606.
8. Loe, D. W., Almquist, K. C., Cole, S. P., and Deeley, R. G. (1996) ATP-dependent 17 beta-estradiol 17-(beta-D-glucuronide) transport by multidrug resistance protein (MRP). Inhibition by cholestatic steroids, *J Biol. Chem. 271*, 9683−9689.
9. Jedlitschky, G., Leier, I., Buchholz, U., Barnouin, K., Kurz, G., and Keppler, D. (1996) Transport of glutathione, glucuronate, and sulfate conjugates by the MRP gene-encoded conjugate export pump, *Cancer Res. 56*, 988−994.
10. Loe, D. W., Stewart, R. K., Massey, T. E., Deeley, R. G., and Cole, S. P. (1997) ATP-dependent transport of aflatoxin B1 and its glutathione conjugates by the product of the multidrug resistance protein (MRP) gene, *Mol. Pharmacol. 51*, 1034−1041.
11. Leier, I., Jedlitschky, G. Buchholz, U., Center, M., Cole, S. P., Deeley, R. G., and Keppler, D. (1999) ATP-dependent glutathione disulphide transport mediated by the MRP gene-encoded conjugate export pump, *Biochem. J 314*, 433−437.
12. Priebe, W., Krawczyk, M., Kuo, M. T., Yamane, Y., Savaraj, N., and Ishikawa, T. (1998) Doxorubicin- and daunorubicin-glutathione conjugates, but not unconjugated drugs, competitively inhibit leukotriene C_4 transport mediated by MRP/GS-X pump, *Biochem. Biophys. Res. Commun. 247*, 859−863.
13. Loe, D. W., Deeley, R. G., and Cole, S. P. (1998) Characterization of vincristine transport by the M(r) 190,000 multidrug resistance protein (MRP): evidence for cotransport with reduced glutathione, *Cancer Res. 58*, 5130−5136.
14. Leslie, E. M., Ito, K., Upadhyaya, P., Hecht, S. S., Deeley, R. G., and Cole, S. P. (2001) Transport of the beta-O-glucuronide conjugate of the tobacco-specific carcinogen 4-(methylnitrosamino)-1-(3-pyridyl)-1-butanol (NNAL) by the multidrug resistance protein 1 (MRP1). Requirement for glutathione or a non-sulfur-containing analogue, *J. Biol. Chem. 276*, 27846−27854.
15. Qian, Y. M., Song, W. C., Cui, H., Cole, S. P., and Deeley, R. G. (2001) Glutathione stimulates sulfated estrogen transport by multidrug resistance protein 1, *J. Biol. Chem. 276*, 6404−6411.
16. Loe, D. W., Almquist, K. C., Deeley, R. G., and Cole, S. P. (1996) Multidrug resistance protein (MRP)-mediated transport of leukotriene C_4 and chemotherapeutic agents in membrane vesicles. Demonstration of glutathione-dependent vincristine transport, *J. Biol. Chem. 271*, 9675−9682.

17. Renes, J., de Vries, E. G., Nienhuis, E. F., Jansen, P. L., and Muller, M. (1999) ATP- and glutathione-dependent transport of chemotherapeutic drugs by the multidrug resistance protein MRP1, *Br. J Pharmacol. 126*, 681−688.
18. Ding, G. Y., Shen, T., and Center, M. S. (1999) Multidrug resistance-associated protein (MRP) mediated transport of daunomycin and leukotriene C_4 (LTC_4) in isolated plasma membrane vesicles, *Anticancer Res. 19*, 3243−3248.
19. Kool, M., de Haas, M., Scheffer, G. L., Scheper, R. J., van Eijk, M. J., Juijn, J. A., Baas, F., and Borst, P. (1997) Analysis of expression of cMOAT (MRP2), MRP3, MRP4, and MRP5, homologues of the multidrug resistance-associated protein gene (MRP1), in human cancer cell lines, *Cancer Res. 57*, 3537−3547.
20. Kool, M., van der, L. M., de Haas, M., Baas, F., and Borst, P. (1999) Expression of human MRP6, a homologue of the multidrug resistance protein gene MRP1, in tissues and cancer cells, *Cancer Res. 59*, 175−182.
21. Hopper, E., Belinsky, M. G., Zeng, H., Tosolini, A., Testa, J. R., and Kruh, G. D. (2001) Analysis of the structure and expression pattern of MRP7 (ABCC10), a new member of the MRP subfamily, *Cancer Lett. 162*, 181−191.
22. Bera, T. K., Lee, S., Salvatore, G., Lee, B., and Pastan, I. (2001) MRP8, a new member of ABC transporter superfamily, identified by EST database mining and gene prediction program, is highly expressed in breast cancer, *Mol. Med. 7*, 509−516.
23. Bera, T. K., Iavarone, C., Kumar, V., Lee, S., Lee, B., and Pastan, I. (2002) MRP9, an unusual truncated member of the ABC transporter superfamily, is highly expressed in breast cancer, *Proc. Natl. Acad. Sci. U.S.A. 99*, 6997−7002.
24. Hipfner, D. R., Almquist, K. C., Leslie, E. M., Gerlach, J. H., Grant, C. E., Deeley, R. G., and Cole, S. P. (1997) Membrane topology of the multidrug resistance protein (MRP). A study of glycosylation-site mutants reveals an extracytosolic NH_2 terminus, *J. Biol. Chem. 272*, 23623−23630.
25. Kast, C., and Gros, P. (1997) Topology mapping of the amino-terminal half of multidrug resistance-associated protein by epitope insertion and immunofluorescence, *J. Biol. Chem. 272*, 26479−26487.
26. Bakos, E., Hegedus, T., Hollo, Z., Welker, E., Tusnady, G. E., Zaman, G. J., Flens, M. J., Varadi, A., and Sarkadi, B. (1996) Membrane topology and glycosylation of the human multidrug resistance-associated protein, *J. Biol. Chem. 271*, 12322−12326.
27. Tusnady, G. E., Bakos, E., Varadi, A., and Sarkadi, B. (1997) Membrane topology distinguishes a subfamily of the ATP-binding cassette (ABC) transporters, *FEBS Lett. 402*, 1−3.
28. Deeley, R. G., and Cole, S. P. (1997) Function, evolution and structure of multidrug resistance protein (MRP), *Semin. Cancer Biol. 8*, 193−204.
29. Grant, C. E., Kurz, E. U., Cole, S. P., and Deeley, R. G. (1997) Analysis of the intron-exon organization of the human multidrug-resistance protein gene (MRP) and alternative splicing of its mRNA, *Genomics 45*, 368−378.
30. Gao, M., Yamazaki, M., Loe, D. W., Westlake, C. J., Grant, C. E., Cole, S. P., and Deeley, R. G. (1998) Multidrug resistance protein. Identification of regions required for active transport of leukotriene C_4, *J. Biol. Chem. 273*, 10733−10740.
31. Bakos, E., Evers, R., Calenda, G., Tusnady, G. E., Szakacs, G., Varadi, A., and Sarkadi, B. (2000) Characterization of the amino-terminal regions in the human multidrug resistance protein (MRP1), *J. Cell Sci. 61*, 4451−4461.
32. Qian, Y. M., Qiu, W., Gao, M., Westlake, C. J., Cole, S. P., and Deeley, R. G. (2001) Characterization of binding of leukotriene C_4 by human multidrug resistance protein 1: Evidence of differential interactions with NH_2- and COOH-proximal halves of the protein, *J. Biol. Chem. 276*, 38636−38644.
33. Bakos, E., Evers, R., Szakacs, G., Tusnady, G. E., Welker, E., Szabo, K., de Haas, M., van Deemter, L., Borst, P., Varadi, A., and Sarkadi, B. (1998) Functional multidrug resistance protein (MRP1) lacking the N-terminal transmembrane domain, *J. Biol. Chem. 273*, 32167−32175.
34. Ren, X. Q., Furukawa, T., Aoki, S., Nakajima, T., Sumizawa, T., Haraguchi, M., Chen, Z. S., Kobayashi, M., and Akiyama, S. (2001) Glutathione-dependent binding of a photoaffinity analogue of agosterol A to the C-terminal half of human multidrug resistance protein, *J. Biol. Chem. 276*, 23197−23206.
35. Daoud, R., Desneves, J., Deady, L. W., Tilley, L., Scheper, R. J., Gros, P., and Georges, E. (2000) The multidrug resistance protein is photoaffinity labeled by a quinoline-based drug at multiple sites, *Biochemistry 39*, 6094−6102.
36. Daoud, R., Kast, C., Gros, P., and Georges, E. (2000) Rhodamine 123 binds to multiple sites in the multidrug resistance protein (MRP1), *Biochemistry 39*, 15344−15352.
37. Daoud, R., Julien, M., Gros, P., and Georges, E. (2001) Major Photoaffinity Drug Binding Sites in Multidrug Resistance Protein 1 (MRP1) Are within Transmembrane Domains 10−11 and 16−17, *J. Biol. Chem. 276*, 12324−12330.
38. Qian, Y. M., Grant, C. E., Westlake, C. J., Zhang, D. W., Lander, P. A., Shepard, R. L., Dantzig, A. H., Cole, S. P., and Deeley, R. G. (2002) Photolabeling of human and murine multidrug resistance protein 1 with the high affinity inhibitor [^{125}I]LY475776 and azidophenacyl-[^{35}S]glutathione, *J. Biol. Chem. 277*, 35225−35231.
39. Mao, Q., Qiu, W., Weigl, K. E., Lander, P. A., Tabas, L. B., Shepard, R. L., Dantzig, A. H., Deeley, R. G., and Cole, S. P. (2002) GSH-dependent photolabeling of multidrug resistance protein MRP1 (ABCC1) by [^{125}I]LY475776. Evidence of a major binding site in the COOH-proximal membrane spanning domain, *J. Biol. Chem. 277*, 28690−28699.
40. Gao, M., Loe, D. W., Grant, C. E., Cole, S. P., and Deeley, R. G. (1996) Reconstitution of ATP-dependent leukotriene C_4 transport by coexpression of both half-molecules of human multidrug resistance protein in insect cells, *J Biol. Chem. 271*, 27782−27787.
41. Wilson, G. M., and Deeley, R. G. (1995) An episomal expression vector system for monitoring sequence-specific effects on mRNA stability in human cell lines, *Plasmid 33*, 198−207.
42. Hipfner, D. R., Gauldie, S. D., Deeley, R. G., and Cole, S. P. (1994) Detection of the M(r) 190,000 multidrug resistance protein, MRP, with monoclonal antibodies, *Cancer Res. 54*, 5788−5792.
43. Hipfner, D. R., Almquist, K. C., Stride, B. D., Deeley, R. G., and Cole, S. P. (1996) Location of a protease-hypersensitive region in the multidrug resistance protein (MRP) by mapping of the epitope of MRP-specific monoclonal antibody QCRL-1, *Cancer Res. 56*, 3307−3314.
44. Hipfner, D. R., Gao, M., Scheffer, G., Scheper, R. J., Deeley, R. G., and Cole, S. P. (1998) Epitope mapping of monoclonal antibodies specific for the 190-kDa multidrug resistance protein (MRP), *Br. J. Cancer 78*, 1134−1140.
45. Flens, M. J., Izquierdo, M. A., Scheffer, G. L., Fritz, J. M., Meijer, C. J., Scheper, R. J., and Zaman, G. J. (1994) Immunochemical detection of the multidrug resistance-associated protein MRP in human multidrug-resistant tumor cells by monoclonal antibodies, *Cancer Res. 54*, 4557−4563.
46. Ciaccio, P. J., Shen, H., Kruh, G. D., and Tew, K. D. (1996) Effects of chronic ethacrynic acid exposure on glutathione conjugation and MRP expression in human colon tumor cells, *Biochem. Biophys. Res. Commun. 222*, 111−115.
47. Kunst, M., Sies, H., and Akerboom, T. P. (1989) S-(4-azidophenacyl)[^{35}S]glutathione photoaffinity labeling of rat liver plasma membrane-associated proteins, *Biochim. Biophys. Acta 982*, 15−23.
48. Eisenberg, D., Schwarz, E., Komaromy, M., and Wall, R. (1984) Analysis of membrane and surface protein sequences with the hydrophobic moment plot, *J. Mol. Biol. 179*, 125−142.
49. Denning, G. M., Anderson, M. P., Amara, J. F., Marshall, J., Smith, A. E., and Welsh, M. J. (1992) Processing of mutant cystic fibrosis transmembrane conductance regulator is temperature-sensitive, *Nature 358*, 761−764.
50. Leslie, E. M., Letourneau, I. J., Deeley, R. G., and Cole, S. P. (2003) Functional and structural consequences of cysteine substitutions in the NH_2 proximal region of the human multidrug resistance protein 1 (MRP1/ABCC1), *Biochemistry 42*, 5214−5224.
51. Ito, K., Weigl, K. E., Deeley, R. G., and Cole, S. P. (2003) Mutation of proline residues in the NH2-terminal region of the multidrug resistance protein, MRP1 (ABCC1): Effects on protein expression, membrane localization and transport function, *Biochim. Biophys. Acta 1615*, 103−114.
52. Krogh, A., Larsson, B., von Heijne, G., and Sonnhammer, E. L. (2001) Predicting transmembrane protein topology with a hidden Markov model: application to complete genomes, *J. Mol. Biol. 305*, 567−580.
53. Locher, K. P., Lee, A. T., and Rees, D. C. (2002) The *E. coli* BtuCD structure: a framework for ABC transporter architecture and mechanism, *Science 296*, 1091−1098.
54. Karwatsky, J., Daoud, R., Cai, J., Gros, P., and Georges, E. (2003) Binding of a photoaffinity analogue of glutathione to MRP1 (ABCC1) within two cytoplasmic regions (L0 and L1) as well as transmembrane domains 10−11 and 16−17, *Biochemistry 42*, 3286−3294.

55. Mikhailov, M. V., Mikhailova, E. A., and Ashcroft, S. J. H. (2001) Molecular structure of the glibenclamide binding site of the beta-cell K_{ATP} channel, *FEBS Lett. 499*, 154−160.
56. Aguilar-Bryan, L., Nichols, C. G., Wechsler, S. W., Clement, J. P., IV, Boyd, A. E., III, Gonzalez, G., Herrera-Sosa, H., Nguy, K., Bryan, J., and Nelson, D. A. (1995) Cloning of the beta cell high-affinity sulfonylurea receptor: a regulator of insulin secretion, *Science 268*, 423−426.
57. Chan, K. W., Zhang, H., and Logothetis, D. E. (2003) N-terminal transmembrane domain of the SUR controls trafficking and gating of Kir6 channel subunits, *EMBO J. 22*, 3833−3843.
58. Fu, J., Ji, H. L., Naren, A. P., and Kirk, K. L. (2001) A cluster of negative charges at the amino terminal tail of CFTR regulates ATP-dependent channel gating, *J. Physiol. 536*, 459−470.
59. Naren, A. P., Cormet-Boyaka, E., Fu, J., Villain, M., Blalock, J. E., Quick, M. W., and Kirk, K. L. (1999) CFTR chloride channel regulation by an interdomain interaction, *Science 286*, 544−548.
60. Peters, K. W., Qi, J., Watkins, S. C., and Frizzell, R. A. (1999) Syntaxin 1A inhibits regulated CFTR trafficking in *Xenopus* oocytes, *Am. J. Physiol. 277*, C174−C180.
61. Naren, A. P., Nelson, D. J., Xie, W., Jovov, B., Pevsner, J., Bennett, M. K., Benos, D. J., Quick, M. W., and Kirk, K. L. (1997) Regulation of CFTR chloride channels by syntaxin and Munc18 isoforms, *Nature 390*, 302−305.
62. Jones, D. T. (1999) Protein secondary structure prediction based on position-specific scoring matrices, *J. Mol. Biol. 292*, 195−202.
63. Geourjon, C., and Deleage, G. (1995) SOPMA: significant improvements in protein secondary structure prediction by consensus prediction from multiple alignments, *Comput. Appl. Biosci. 11*, 681−684.
64. Rost, B., and Sander, C. (1993) Prediction of protein secondary structure at better than 70% accuracy, *J. Mol. Biol. 232*, 584−599.

BI035333Y